Field dynamics, instabilities, and phase squeezing in the two-photon correlated-emission laser

J. Bergou, J. Zhang, and C. Su
Department of Physics, Hunter College of the City University of New York, 695 Park Avenue, New York, New York 10021
(Received 27 July 1994; revised manuscript received 27 March 1995)

Both stationary and time-dependent regimes of operation, instabilities, and phase squeezing are investigated in the off-resonant two-photon correlated-spontaneous-emission laser by numerical calculation. Initial atomic coherence plays an essential role in lasing without population inversion, phase locking, and phase noise squeezing in the system. Under certain conditions, in the inverted and noninverted regimes alike, the output intensity exhibits bistable behaviors against the initial atomic coherence. Depending on the parameters, the whole or a portion of the upper or lower branch gives stable operations. In the inverted regime, even tristable behavior can be found in a narrow range of parameters. The field evolution and dynamics are studied. Furthermore, phase noise reduction near bistable areas is also investigated. In addition to the lower branch, where from previous studies, it has been known to exist, phase squeezing is also found on the upper branch both with and without population inversion, thus generating a bright source of phase noise squeezed light.

PACS number(s): 42.50.Dv, 42.50.Lc, 42.65.Pc

I. INTRODUCTION

Recently much attention has been paid to the laser with injected atomic coherence as an attractive candidate to achieve phase and frequency locking as well as noise suppression [1]. In a previous paper [2], we analyzed the influence of the injected atomic coherence on ordinary single-photon laser operation and noise quenching. Both steady-state and time-dependent regimes were investigated. We gave a detailed discussion of regimes with and without phase locking. The purpose of the present paper is to provide a similar analysis for the two-photon laser with injected atomic coherence.

Since the beginning of the theoretical research on squeezing in the laser, the problem of squeezed-state generation in two-photon systems has attracted much attention. An early work by Yuen [3] suggested the two-photon laser as a potential candidate for generating squeezed states of the radiation field. Later, it was shown [4] that due to the spontaneous-emission noise any possible squeezing at steady state would be destroyed and only transient squeezing becomes possible [5]. Recent work, including both linear [6–9] and nonlinear [10,11] theory, has extended the investigations to coherent initial conditions in this two-photon system: if the atoms are pumped into an appropriate superposition of the lasing states, quenching of spontaneous-emission noise may occur. In this way, it has been shown that the generation of squeezed light is compatible with gain [6,7] and even with atomic inversion by adding an additional lower level [8] or by choosing a fast decaying intermediate relay level [9], thus providing bright sources of squeezed light.

In the present paper, we study the field dynamics, instability, and phase noise fluctuations of the two-photon correlated-emission laser (CEL) as functions of the various detunings (cavity field, atom field) and atomic coherence numerically. We consider the simple off-resonant two-photon CEL scheme [6,7] with the middle level unpopulated. Nonlinear theory is adopted in the calculation. It is shown that, similar to the case of the one-photon CEL, the steady-state solution exhibits bistability of intensity against initial atomic coherence, population inversion is no longer necessary to maintain lasing, and initial atomic coherence provides phase locking. The essential difference between this system and the one-photon CEL is that there exists a threshold, below which the lower branch of the bistable intensity is always zero. In addition, tristable behavior can be found in the two-photon CEL. We study the field dynamics and instabilities with limit cycle behavior. We then investigate the effect of initial atomic coherence on noise. Besides showing that phase noise can be squeezed on the lower branch, we find that the phase noise squeezing persists on the upper branch for the noninverted regime and, more importantly, even for the inverted regime. We therefore obtain a bright source of squeezed light in the simple two-photon CEL scheme without the need of additional lower level or the fast decaying intermediate relay level.

This paper is organized in the following way. In Sec. II we start with the Fokker-Planck equation developed in Refs. [10] and [11] to derive a set of nonlinear differential equations and discuss the steady-state operation and stability. In Sec. III, we study the time evolution and the field dynamics. In Sec. IV, using moments of Q distribution, we calculate numerical solutions for the steady-state noise. Finally, Sec. V summarizes the findings of the paper.

II. FOKKER-PLANCK EQUATION

We consider a system of three-level atoms, as shown in Fig. 1, interacting with a single-mode field of frequency ν. The Hamiltonian for the system, in the rotating-wave approximation, is given by

$$H = H_{\text{at}} + H_F + H_{\text{int}} , \tag{2.1}$$

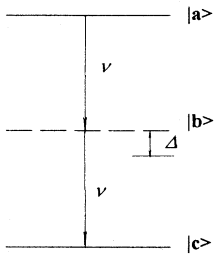

FIG. 1. Atomic levels relevant to the two-photon CEL. Atoms are injected in a coherent superposition of levels $|a\rangle$ and $|c\rangle$, with no initial population in level $|b\rangle$.

where $H_{\rm at}$, H_F, and $H_{\rm int}$ are, respectively, the atom, field, and interaction terms with

$$H_{\rm at}=\sum_{j=a,b,c}\hbar\omega_j|j\rangle\langle j|\ , \tag{2.2}$$

$$H_F=\hbar\Omega(a^\dagger a+\tfrac{1}{2})\ , \tag{2.3}$$

$$H_{\rm int}=\hbar g_{ab}(a|a\rangle\langle b|+a^\dagger|b\rangle\langle a|)+\hbar g_{bc}(a|b\rangle\langle c|+a^\dagger|c\rangle\langle b|)\ . \tag{2.4}$$

Here a and $a^\dagger$ are the field annihilation and creation operators, respectively; Ω is the cavity-mode frequency; $\hbar\omega$ is the energy of level i and $|i\rangle$ are the atomic states ($i=a,b,c$); g_{ab} and g_{bc} are the coupling constants for the transitions $|a\rangle\rightarrow|b\rangle$ and $|b\rangle\rightarrow|c\rangle$, respectively (for simplicity, from now on we consider $g_{ab}=g_{bc}=g$). We have assumed that only the $|a\rangle\rightarrow|b\rangle$ and $|b\rangle\rightarrow|c\rangle$ transitions are allowed. We consider the case that the atoms are injected into the laser cavity with initial populations $\rho^j_{aa}(t_j)=\rho_{aa}$ and $\rho^j_{cc}(t_j)=\rho_{cc}$ ($=1-\rho_{aa}$) and initial coherence between the top and bottom levels $\rho^j_{ac}(t_j)=\rho^j_{ca}(t_j)^*=\bar\rho_{ac}\exp(-2i\nu t_j)$. The middle level b is unpopulated. The atomic injection rate is r_a.

In Q representation this system can be described with a Fokker-Planck equation (Ref. [11]). If we introduce the scaled intensity and phase variables, n and φ, the Fokker-Planck equation becomes

$$\frac{\partial Q(n,\varphi)}{\partial\bar t}=\left[-\frac{\partial}{\partial n}d_n-\frac{\partial}{\partial\varphi}d_\varphi+\eta\frac{\partial^2}{\partial n^2}D_{nn}+\eta\frac{\partial^2}{\partial\varphi^2}D_{\varphi\varphi}+2\eta\frac{\partial^2}{\partial n\,\partial\varphi}D_{n\varphi}\right]Q(n,\varphi)\ , \tag{2.5}$$

with

$$d_n=\frac{n[G(1+n)-2\delta C\sin2\varphi]}{(1+n)^2+\delta^2}-n\ , \tag{2.6}$$

$$d_\varphi=D-\frac{\delta[\tilde\alpha+2C\cos2\varphi]}{2(1+4n+\delta^2)}\ , \tag{2.7}$$

$$D_{nn}=n\left[\frac{(1+n)(2\tilde\alpha-G)+2\delta C\sin2\varphi}{2[(1+n)^2+\delta^2]}-\frac{\tilde\alpha+2C\cos2\varphi}{2[1+4n+\delta^2]}+\frac{nG[(1+n)^2-\delta^2]-4n\delta(1+n)C\sin2\varphi}{[(1+n)^2+\delta^2]^2}\right]+n\ , \tag{2.8}$$

$$D_{\varphi\varphi}=\left[\frac{-(1+n)G+2\delta C\sin2\varphi}{8[(1+n)^2+\delta^2]}+\frac{(2C\cos2\varphi+\tilde\alpha)(1+4n)-4\delta C\sin2\varphi}{8[1+4n+\delta^2]}\right]+\frac{1}{4n}\ , \tag{2.9}$$

$$D_{n\varphi}=\frac{1}{4}\left[\frac{\delta G+2\delta C\cos2\varphi+2C\sin2\varphi}{(1+n)^2+\delta^2}-\frac{4\delta n(\tilde\alpha+2C\cos2\varphi)}{[1+4n+\delta^2]^2}-\frac{2\delta(1+n)nG+4n\delta^2C\sin2\varphi}{[(1+n)^2+\delta^2]^2}-\frac{\delta G}{1+4n+\delta^2}\right]\ , \tag{2.10}$$

where

$$G=\frac{\alpha(\rho_{aa}-\rho_{cc})}{\gamma}\ ,$$

$$n=\frac{\beta I}{2\alpha}\ ,$$

$$C=\frac{\alpha|\bar\rho_{\rm ac}|}{\gamma}\ ,$$

$$D=\frac{\nu-\Omega}{\gamma}\ ,$$

$$\delta=\frac{\Delta}{\Gamma}\ ,$$

$$\eta=\frac{\beta}{2\alpha}\ ,$$

and

$$\bar t=t\gamma\ ,$$

$\tilde\alpha=(\alpha/\gamma)$ (with I equal to the photon number). Here $\alpha=[(2r_ag^2)/(\Gamma^2)]$ is a linear-gain coefficient, $\beta=[(8r_ag^4)/(\Gamma^4)]$ saturation parameter, Γ is the atomic decay rate (for simplicity assumed to be the same for all levels, $\Gamma_a=\Gamma_b=\Gamma_c=\Gamma$), and γ is the cavity-loss rate. We have introduced $\varphi=\phi-\frac{1}{2}\theta_{\rm ac}$, where ϕ is the phase of the laser field and $\theta_{\rm ac}$ is the phase of atomic coherence. Furthermore, D is the cavity-field detuning, δ is the atom-field detuning [$\Delta=\omega_{ab}-\nu=-(\omega_{bc}-\nu)$, i.e., overall two-photon resonance is assumed].

In a steady state we obtain the following set of coupled nonlinear equations for the intensity n_0 and phase φ_0,

$$d_n=\frac{n_0[G(1+n_0)-2\delta C\sin 2\varphi_0]}{(1+n_0)^2+\delta^2}-n_0=0\ , \tag{2.11}$$

$$d_\varphi=D-\frac{\delta[\tilde{\alpha}+2C\cos 2\varphi_0]}{2(1+4n_0+\delta^2)}=0\ . \tag{2.12}$$

After eliminating the phase φ_0 we can find a fifth-order equation for n_0,

$$n_0\{n_0^4+(4-2G)n_0^3+[64D^2+2\delta^2+G^2-6G+6]n_0^2+[(4-2G)(1+\delta^2-G)-16D(\delta\tilde{\alpha}-2D-2D\delta^2)]n_0+[(1+\delta^2-G)^2+(\delta\tilde{\alpha}-2D-2D\delta^2)^2-4\delta^2C^2]\}=0\ , \tag{2.13a}$$

where one solution is always

$$n_0=0\ . \tag{2.13b}$$

From Eqs. (2.13a) and (2.13b) the steady-state curve of intensity n_0 as a function of the atomic coherence C is multivalued for some set of parameters. This multistable behavior is different from that of the one-photon correlated-spontaneous-emission laser. One of the obvious differences is that the lower branch is always $n_0=0$. Another significant difference is that the first derivative at the threshold point $C_{\rm th}$ is not continuous.

Using linear-stability analysis, we can find the stability conditions for the steady state (for details see Ref. [2]):

$$\left[\frac{\partial d_n}{\partial n}\right]_0+\left[\frac{\partial d_\varphi}{\partial\varphi}\right]_0\le 0\ , \tag{2.14}$$

$$\left[\frac{\partial d_n}{\partial n}\right]_0\left[\frac{\partial d_\varphi}{\partial\varphi}\right]_0-\left[\frac{\partial d_\varphi}{\partial n}\right]_0\left[\frac{\partial d_n}{\partial\varphi}\right]_0\ge 0\ . \tag{2.15}$$

The subscript 0 means that the derivatives have to be evaluated in the steady state. We find that for the lower branch, $n_0=0$, condition (2.14) reads

$$G\le 1+\delta^2\ , \tag{2.16}$$

and condition (2.15) yields

$$\left[\frac{G-2\delta C\sin 2\varphi_0}{1+\delta^2}-1\right]\cdot\frac{2\delta C\sin 2\varphi_0}{1+\delta^2}\ge 0\ . \tag{2.17}$$

We can also find the phase locking condition from Eq. (2.12) (following the standard analysis of Ref. [12]):

$$|2C\delta|\ge|2D(1+\delta^2)-\delta\tilde{\alpha}|\ , \tag{2.18}$$

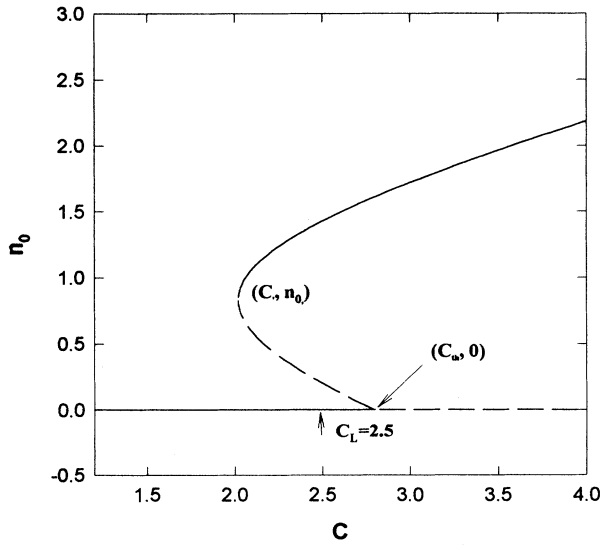

FIG. 2. Steady-state scaled intensity n_0 as a function of initial atomic coherence C with $G=0$, $D=1$, $\delta=2$, and $\tilde{\alpha}=10$. The solid line corresponds to the stable steady state and the dashed line corresponds to the unstable steady state.

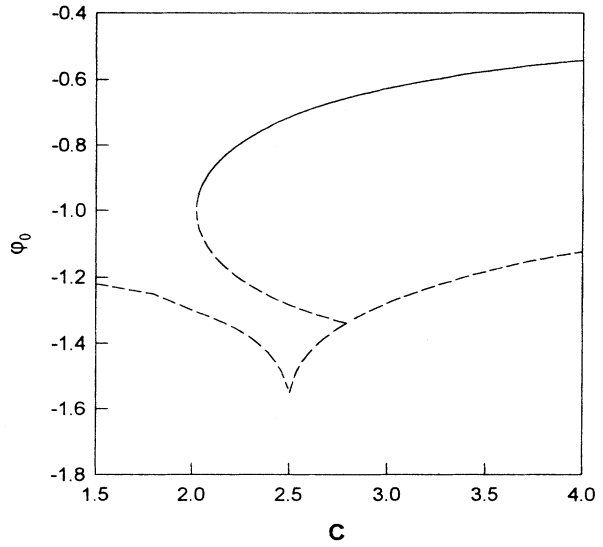

FIG. 3. Steady-state phase φ_0 as a function of C with the same parameters as in Fig. 2.

and the threshold point from Eq. (2.13a) assuming $n_0=0$

$$(1+\delta^2-G)^2+(\delta\tilde{\alpha}-2D-2D\delta^2)^2-4\delta^2C_{\rm th}^2=0\ . \qquad (2.19)$$

In Fig. 2, we plot the bistability curve of the intensity n_0 as a function of the atomic coherence C with $G=-2.0$, $D=1.0$, $\delta=2.0$, and $\tilde{\alpha}=10$. The phase φ_0 as a function of C is presented in Fig. 3 with parameters being the same as in Fig. 2. The physically accessible region is given by $0\le C\le\tilde{\alpha}\sqrt{\rho_{aa}\rho_{cc}}$, which, for the given parameters, is $0\le C\le 5$. For nonzero solutions [the steady state satisfies Eq. (2.13a)] condition (2.15) leads to $(\partial n/\partial C)\ge 0$. This means that the parts of the curve with negative slope are unstable (in the n-C plane). The upper turning point (C_T,n_{0T}) of the multivalued steady state satisfies

$$2n_0^3+3(2-G)n_0^2+(64D^2+2\delta^2+G^2-6G+6)n_0+(2-G)(1+\delta^2-G)-8D(\delta\tilde{\alpha}-2D-2D\delta^2)=0\ . \qquad (2.20)$$

For the particular set of parameters of Figs. 2 and 3 we find the phase-locking point $C_L=2.5$, upper turning point $C_T=2.0$, and threshold point $C_{\rm th}=2.8$. In the subregion $0\le C\le 2.0$ there is only one steady state, $n_0=0$, and it is stable, but the phase φ_0 is unlocked. In the subregion $2.0\le C\le 2.5$, there are three curves: the upper branch with positive slope, the middle branch with negative slope, and the lower branch, $n_0=0$. We know that the part with negative slope is unstable and the other two branches are stable. The time evolution $n(\bar{t})$ exhibits different behavior for different initial regions, separated by the middle section. Starting from a value below middle section, $n(\bar{t})$ will reach $n_0=0$. If the initial value is above the middle section, $n(\bar{t})$ will finally reach the upper branch. The phase φ_0 for the upper branch is locked and the phase φ_0 for the lower branch $n_0=0$ is unlocked. For $2.5\le C\le 2.8$, intensity versus time behavior is similar to that in previous region, but the phase for $n_0=0$ is locked to a particular value. Above $C_{\rm th}$, only the upper branch is stable. This dynamical feature is similar to that in a system of an optical parametric oscillator coupled to N two-level atoms [13] and detuned degenerate four-wave mixing [14].

In Fig. 4, we present n_0 as a function of C for another situation. In this case, the whole physics region is given by $0\le C\le 4.68$. Under $C=2.4$, there is no stable curve. In this unstable region, the time-dependent behavior is similar to that in the unstable region of the one-photon correlated-spontaneous-emission laser [2]: $n(\bar{t})$ oscillates around a value which is very close to the critical intensity $n_c=1.3$ after the initial transients have decayed. For the phase $\varphi(\bar{t})$, superimposed on a straight line which is represented by the average slope of the phase versus time curve, there is a small oscillation very similar to the oscil-

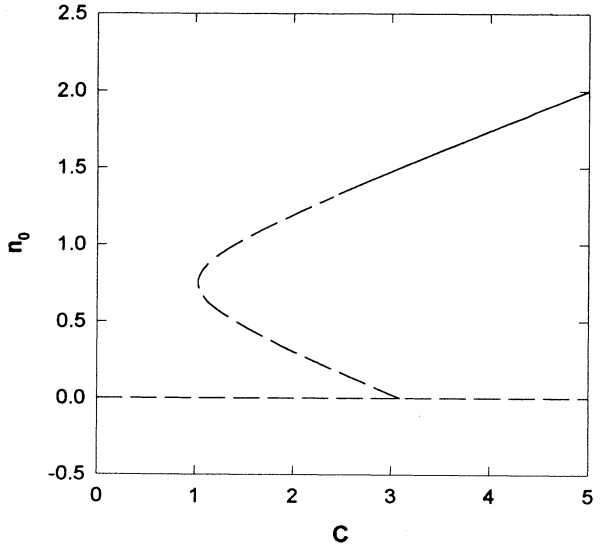

FIG. 4. Steady-state scaled intensity n_0 as a function of initial atomic coherence C with $G=3.5$, $D=1$, $\delta=1$, and $\tilde{\alpha}=10$. The solid line corresponds to the stable steady state and the dashed line corresponds to the unstable steady state.

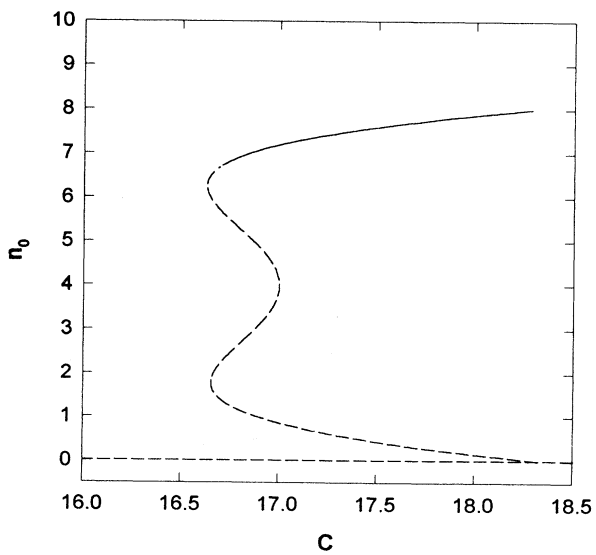

FIG. 5. Steady-state scaled intensity n_0 as a function of initial atomic coherence C with $G=10$, $D=0.78$, $\delta=0.72$, and $\tilde{\alpha}=38$. The solid line corresponds to the stable steady state and the dashed line corresponds to the unstable steady state.

lation of the average intensity.

Since Eq. (2.11) is a quintic equation, one naturally expects to obtain the tristable behavior by properly choosing the parameters. Indeed, Fig. 5 shows such situation where the physical region is given by $0 \leq C \leq 18.33$. For $C < 16.65$, there is only one solution $n_0 = 0$ which is unstable. In the region $16.70 \leq C \leq 17.00$, there are five positive solutions, i.e., we have a possibility of tristable operation in this regime. Among them only the top branch is stable. In the region $17.0 \leq C \leq 18.33$, there are three positive solutions, and still only the top level is stable.

III. DYNAMICAL EVOLUTION

So far, we have dealt with the steady states of the system. Let us now consider time-dependent scenarios by keeping the full time dependence in the equations. In this section we will investigate time evolution from a given initial condition. We will first study how the system approaches steady state in those regions of the external control parameters where they exist. Then we will investigate the states that evolve from a given initial state in the unstable regions.

For the time-dependent case, the equations of motion are

$$\frac{dn}{d\bar{t}} = d_n \tag{3.1}$$

and

$$\frac{d\varphi}{d\bar{t}} = d_\varphi \ . \tag{3.2}$$

The nonlinear dynamics of the system is completely determined by Eqs. (3.1) and (3.2).

Before studying the transients around stable steady states, let us first get some analytical insight into the relaxation dynamics by studying the trajectories in the n-φ plane. By transforming equations (3.1) and (3.2) to the form

$$\frac{dn}{d\varphi} = \frac{d_n}{d_\varphi} \tag{3.3}$$

we can obtain the governing equation. Since the time $\bar{t}$ does not appear explicitly in this equation, we can exhibit the integral curves in the n-φ plane. Each point (n,φ) in this plane represents a possible set of initial conditions. A trajectory going through this particular point then determines the time evolution of the system, starting from this initial condition. In Figs. 6–8 we plot the intensity n versus phase φ for several cases. The steady states now correspond to attractive singular points. In Fig. 6, we plot n versus φ with $G=0$, $D=1$, $\delta=2$, $\bar{\alpha}=10$, and $C=2.6$. Points a and b correspond to the stable upper branch and stable lower branch ($n_0=0$), respectively. Depending on the initial conditions, the point $[n(\bar{t}),\varphi(\bar{t})]$ moves, with the increase of the time $\bar{t}$, along the integral curve and converges to the stable point a or b.

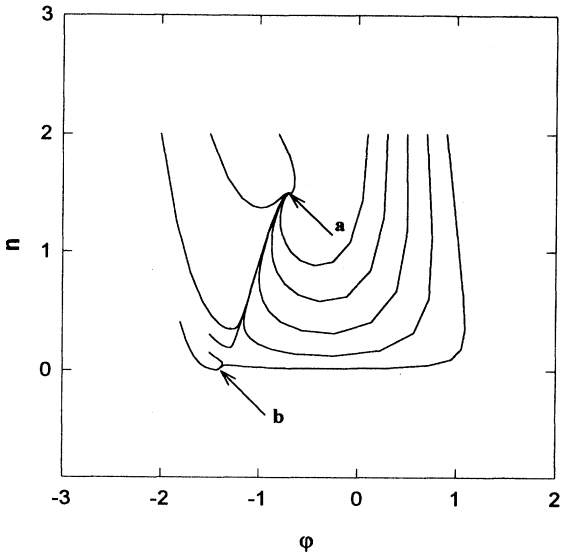

FIG. 6. n-φ trajectories for $G=0$, $D=1.0$, $\delta=2$, $\bar{\alpha}=10$, and $C=2.6$.

Now we discuss time evolution from a given initial condition in those regions of the external control parameters where the steady state becomes unstable, i.e., beyond the critical point. We find that $n(\bar{t})$ oscillates around a value which is very close to the critical intensity, n_c, after the initial transients have decayed. The period of oscillations T can be found from

$$T = \int_0^{2\pi} \frac{d\varphi}{a - b\cos\varphi} = \frac{2\pi}{(a^2 - b^2)^{1/2}} \ , \tag{3.4}$$

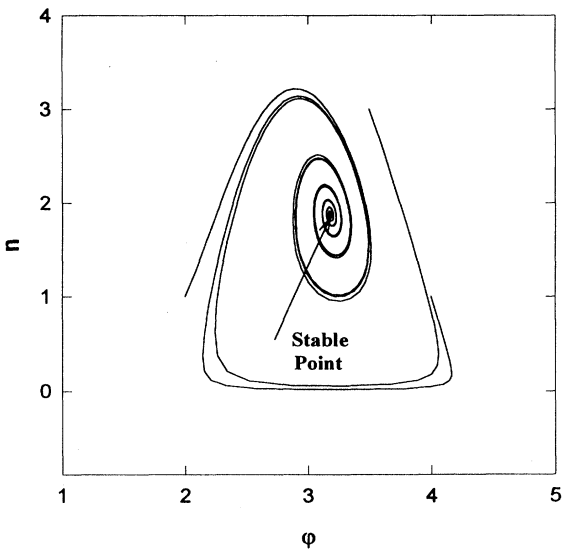

FIG. 7. n-φ trajectories for $G=3.5$, $D=1.0$, $\delta=1$, $\bar{\alpha}=10$, and $C=4.5$.

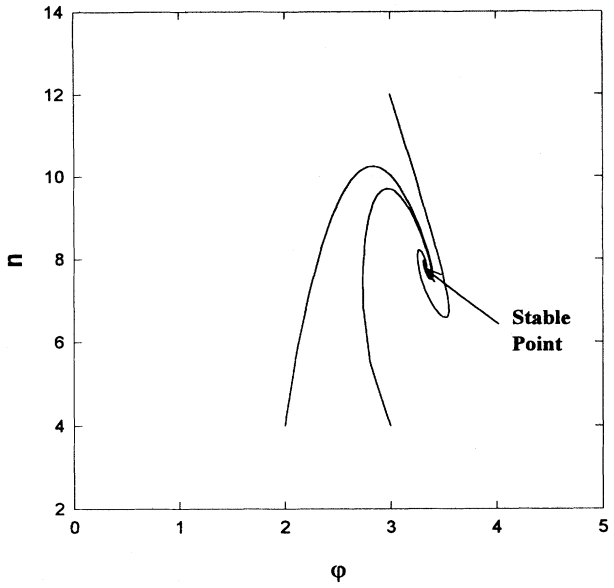

FIG. 8. n-φ trajectories for $G=10$, $D=0.78$, $\delta=0.72$, $\tilde{\alpha}=38$, and $C=18$.

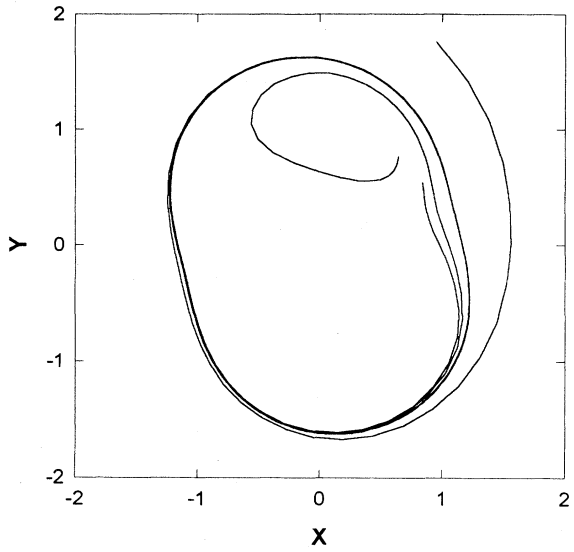

FIG. 10. Integral curves in the phase plane of quadratures, X and Y, with $G=3.5$, $D=1.0$, $\delta=1.0$, $\tilde{\alpha}=10$, and $C=2.0$.

where

$$a=D-\frac{\delta\tilde{\alpha}}{2(1+n_c+\delta^2)}$$

and

$$b=\frac{\delta C}{1+n_c+\delta^2}\ .$$

The phase $\varphi(\bar{t})$ versus $\bar{t}$ is depicted in Fig. 9 with

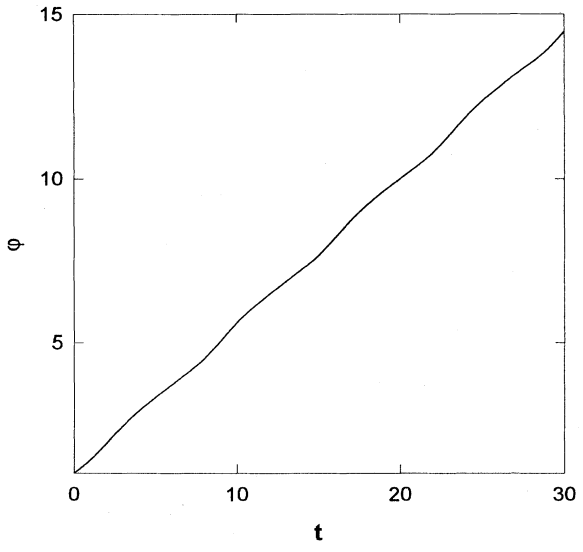

FIG. 9. Time evolution of the phase φ with $G=3.5$, $D=1.0$, $\delta=1.0$, $\tilde{\alpha}=10$, and $C=2.5$.

$G=3.5$, $D=1$, $\delta=1$, $\tilde{\alpha}=10$, and $C=2.5$. The time dependence has two ingredients. First, there is a constant shift of the operating frequency which results in a steady increase of the phase, strictly proportional with time. This is represented by the average slope of the phase versus time curve. Second, superimposed on this straight line evolution, there is a small oscillation very similar to the oscillation of the average intensity. In particular, the frequency of these phase oscillations is the same as that of the intensity oscillations, given by Eq. (3.4).

We next display this oscillatory behavior from another point of view. Namely, we again discuss the integral curves, resulting from Eq. (3.3). This time, however, instead of displaying the trajectories in the $n-\varphi$ plane, we will plot them in the X-Y phase plane of quadratures, where $X=\sqrt{n_0}\cos\varphi_0$ and $Y=\sqrt{n_0}\sin\varphi_0$ are the usual quadrature component variables. Figure 10 shows the trajectories in the X-Y plane with $G=3.5$, $D=1$, $\delta=1$, $\tilde{\alpha}=10$, and $C=2.0$. Each trajectory approaches a stable limit cycle. The point $[X(\bar{t}), Y(\bar{t})]$ starting from any initial condition, after the initial transients, i.e., after the approach to the limit cycle, moves along the limit cycle as $\bar{t}$ increases. The period required for the point to complete one cycle is given by (3.4).

IV. NOISE SQUEEZING IN THE LOCKED REGION

In this section, we will use the Fokker-Planck equations (2.5)–(2.10) to study intensity noise $\langle(\Delta n)^2\rangle$ and phase noise $\langle(\Delta\varphi)^2\rangle$ in the phase-locked region. From the Fokker-Planck equation, we can get an infinite set of coupled ordinary differential equations for the moments of the distribution. If we assume the noise to be weak, $\eta\ll 1$, we can truncate these equations into a finite set of nonlinear equations. In this paper we assume that only

the first- and second-order moments are nonzero. These nonzero moments obey the following equations:

$$\frac{d}{d\bar{t}}\langle n\rangle=\langle d_n\rangle\ , \tag{4.1}$$

$$\frac{d}{d\bar{t}}\langle\varphi\rangle=\langle d_\varphi\rangle\ , \tag{4.2}$$

$$\frac{d}{d\bar{t}}\langle(\delta n)^2\rangle=2\langle d_n\delta n\rangle+2\eta\langle D_{nn}\rangle\ , \tag{4.3}$$

$$\frac{d}{d\bar{t}}\langle(\delta\varphi)^2\rangle=2\langle d_\varphi\delta\varphi\rangle+2\eta\langle D_{\varphi\varphi}\rangle\ , \tag{4.4}$$

$$\frac{d}{d\bar{t}}\langle(\delta n)(\delta\varphi)\rangle=\langle d_n\delta\varphi\rangle+\langle d_\varphi\delta n\rangle+2\eta\langle D_{n\varphi}\rangle\ . \tag{4.5}$$

Here we introduced the notations $\delta n=n-\langle n\rangle$, $\delta\varphi=\varphi-\langle\varphi\rangle$. In the following we discuss the steady-state variances of the intensity and phase. In the Q representation, the intensity variance is

$$\langle(\Delta I)^2\rangle=\langle(\delta I)^2\rangle-\langle I\rangle\ , \tag{4.6}$$

and the phase variance is

$$\langle(\Delta\varphi)^2\rangle=\langle(\delta\varphi)^2\rangle-\frac{1}{4\langle I\rangle}\ , \tag{4.7}$$

where $(\delta\ldots)$ corresponds to the antinormally ordered part of $(\Delta\ldots)$.

Expanding d_n, d_φ, D_{nn}, $D_{n\varphi}$, and $D_{\varphi\varphi}$ around the steady state, n_0 and φ_0, up to the first order in δn and $\delta\varphi$, we get

$$\frac{d}{d\bar{t}}\langle(\delta n)^2\rangle=2\left[\frac{d}{dn}d_n\right]_0\langle(\delta n)^2\rangle+2\left[\frac{d}{d\varphi}d_n\right]_0\langle(\delta n)(\delta\varphi)\rangle+2\eta(D_{nn})_0\ , \tag{4.8}$$

$$\frac{d}{d\bar{t}}\langle(\delta\varphi)^2\rangle=2\left[\frac{d}{d\varphi}d_\varphi\right]_0\langle(\delta\varphi)^2\rangle+2\left[\frac{d}{dn}d_\varphi\right]_0\langle(\delta n)(\delta\varphi)\rangle+2\eta(D_{\varphi\varphi})_0\ , \tag{4.9}$$

$$\frac{d}{d\bar{t}}\langle(\delta n)(\delta\varphi)\rangle=\left\{\left[\frac{d}{dn}d_n\right]_0+\left[\frac{d}{d\varphi}d_\varphi\right]_0\right\}\langle(\delta n)(\delta\varphi)\rangle+\left[\frac{d}{dn}d_\varphi\right]_0\langle(\delta n)^2\rangle+\left[\frac{d}{d\varphi}d_n\right]_0\times\langle(\delta\varphi)^2\rangle+2\eta\langle Dn\varphi\rangle_0\ . \tag{4.10}$$

For the lower branch the steady state is $n_0=0$, and we obtain the following expressions for the diffusion coefficients from Eqs. (2.8)–(2.10):

$$D_{nn}(n_0=0)=n_0\frac{0.5\tilde{\alpha}(1-G)-C\cos2\varphi+\delta C\sin2\varphi}{1+\delta^2}+n_0\ , \tag{4.11}$$

$$D_{\varphi\varphi}(n_0=0)=\frac{1}{4n}\left[\frac{-G+2C\cos2\varphi-2\delta C\sin2\varphi+\tilde{\alpha}}{2(1+\delta^2)}+1\right]\ , \tag{4.12}$$

$$D_{n\varphi}(n_0=0)=\frac{\delta C\cos2\varphi+C\sin2\varphi}{2(1+\delta^2)}\ . \tag{4.13}$$

At threshold, $C=C_{\rm th}$, the phase diffusion coefficient becomes

$$D_{\varphi\varphi}(n_0=0)=\frac{1}{4n_0}\left[\frac{-G}{1+\delta^2}+\frac{3}{2}+\frac{D}{\delta}\right]\ , \tag{4.14}$$

where we have used the threshold condition (2.19). In view of Eq. (4.14), it is obvious that the field-cavity detuning D will increase phase noise. Recall that in the phase-locking equation (2.18), D can play the role of a locking term in some cases. For example, if we choose $G=-2$, $\delta=2$, $\tilde{\alpha}=1$, and increase D, from (4.14) we find $D_{\varphi\varphi}$ increasing, but at the same time, from Eq. (2.18), the phase-locked region increases.

By setting $d/dt=0$ in equations (4.8), (4.9), and (4.10) and solving for $\langle(\delta n)^2\rangle$ and $\langle(\delta\varphi)^2\rangle$, then inserting these into (4.6) and (4.7), we can get

$$\frac{\langle(\Delta I)^2\rangle}{I}=\frac{D_2(D_2D_{22}-D_4D_{11}-2D_3D_{12})+D_3(D_1+D_3)D_{11}}{n(D_1+D_3)(D_2D_4-D_1D_3)}-1 \tag{4.15}$$

and

$$\langle(\Delta\varphi)^2\rangle I=n\frac{D_4(D_4D_{11}-D_2D_{22}-2D_1D_{12})+D_1(D_1+D_3)D_{22}}{(D_1+D_3)(D_2D_4-D_1D_3)}-\frac{1}{4}\ . \tag{4.16}$$

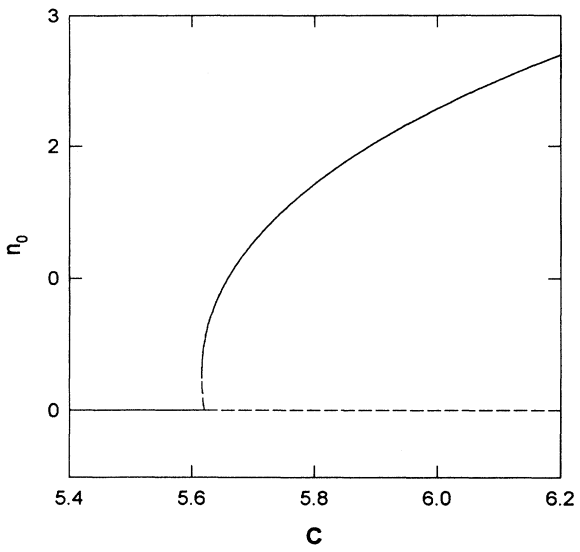

FIG. 11. Steady-state scaled intensity n_0 as a function of initial atomic coherence C with $G=-1$, $D=0.2$, $\delta=4$, and $\bar{\alpha}=12$. The solid line corresponds to the stable steady state, and the dashed line corresponds to the unstable steady state.

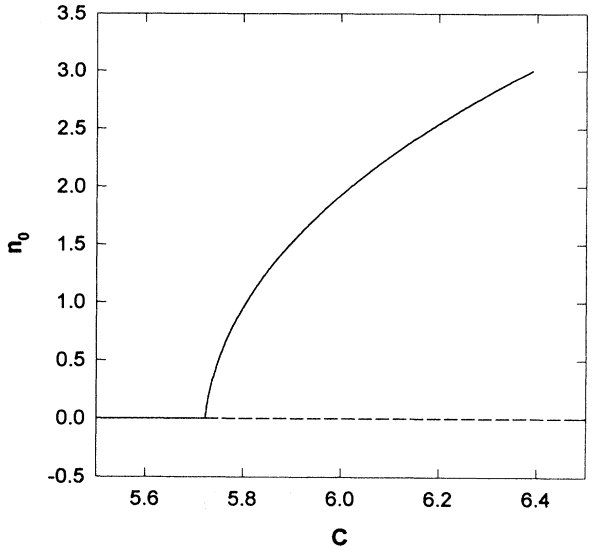

FIG. 13. Steady-state scaled intensity n_0 as a function of initial atomic coherence C with $G=-1$, $D=0.2$, $\delta=6.0$, and $\bar{\alpha}=12$. The solid lines corresponds to the stable steady state and the dashed line corresponds to the unstable steady state.

Here we introduced the notation $D_1=(\partial d_n/\partial n)_0$, $D_2=(\partial d_n/\partial\varphi)_0$, $D_3=(\partial d_\varphi/\partial\varphi)_0$, $D_4=(\partial d_\varphi/\partial n)_0$ and $D_{11}=(d_{nn})_0$, $D_{12}=(D_{n\varphi})_0$, $D_{22}=(D_{\varphi\varphi})_0$ (all quantities are supposed to be taken at the steady state).

We choose three typical sets of parameters to explore the phase squeezing of quantum noise in the two-photon CEL. The steady-state operation and the corresponding phase noise with these two sets of parameters are plotted in Figs. 11–16.

A particular bistable curve related to steady-state equation (2.13) with $G=-1.0$, $D=0.2$, $\delta=4.0$, and $\bar{\alpha}=12.0$ is given in Fig. 11. Below the threshold point, $C_{\text{th}}=5.62$, the lower branch (I) $n_0=0$ is stable and phase locking occurs at $C_L=5.15$. The middle branch (II) is unstable. The whole upper branch (III) is stable and phase is

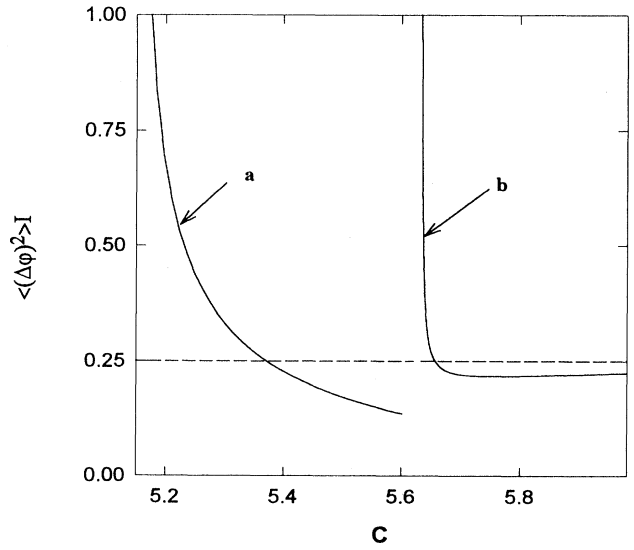

FIG. 12. (a) Steady-state phase noise $\langle(\Delta\varphi)^2\rangle I$ as a function of C from the lower branch in Fig. 11. (b) Steady-state phase noise $\langle(\Delta\phi)^2\rangle I$ as a function of C for the upper branch in Fig. 11. The dashed line corresponds to the shot-noise limit.

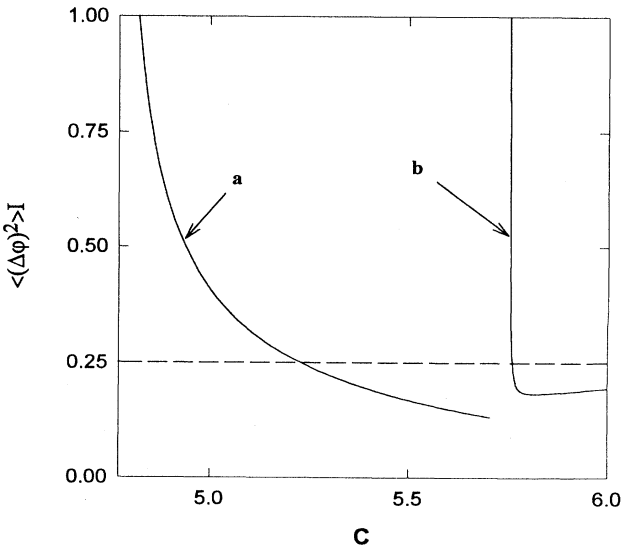

FIG. 14. (a) Steady-state phase noise $\langle(\Delta\varphi)^2\rangle I$ as a function of C for the lower branch in Fig. 13. (b) Steady-state phase noise $\langle(\Delta\varphi)^2\rangle I$ as a function of C for the upper branch in Fig. 13. The dashed line corresponds to the shot-noise limit.

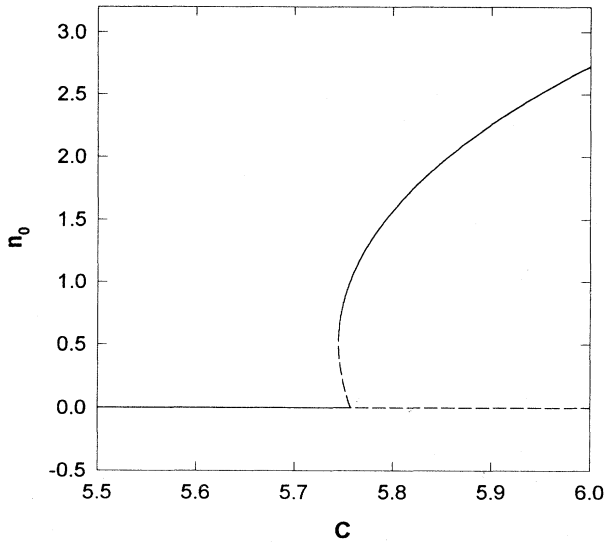

FIG. 15. Steady-state scaled intensity n_0 as a function of initial atomic coherence C with $G=1$, $D=0.2$, $\delta=7$, and $\tilde{\alpha}=12$. The solid line corresponds to the stable steady state and the dashed line corresponds to the unstable steady state.

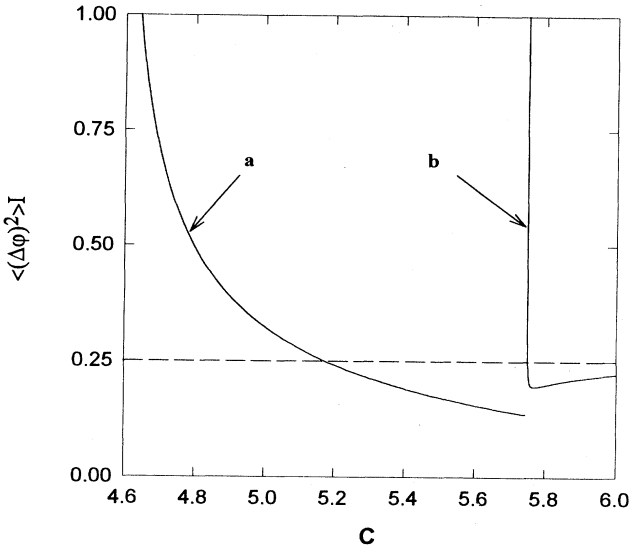

FIG. 16. (a) Steady-state phase noise $\langle(\Delta\varphi)^2\rangle I$ as a function of C for the lower branch in Fig. 15. (b) Steady-state phase noise $\langle(\Delta\varphi)^2\rangle I$ as a function of C for the upper branch in Fig. 15. The dashed line corresponds to the shot-noise limit.

locked. We plot the scaled phase noise $\langle(\Delta\varphi)^2\rangle I$ for the lower branch (I) and upper branch (III) of Fig. 11 versus initial atomic coherence C in Fig. 12. First we see that there is 40% phase squeezing in the lower branch. More importantly, we find nearly 15% phase squeezing for almost the whole physical region of the upper branch except the large noise at the threshold point. Since this squeezing occurs at the upper branch with finite intensity, we therefore have obtained a bright squeezing.

In Fig. 13, we display the intensity n_0 as a function of C with $G=-1.0$, $D=0.2$, $\delta=6.0$, and $\tilde{\alpha}=12$. In this case, there are still two stable branches under stationary operating conditions even though the S-shaped bistable hysteresis no longer exists. The stable and phase-locked region for the lower branch (I) starts from $C_L=4.77$ to $C_{\rm th}=5.72$. The plots of the phase noise as a function of C for the lower branch (I) and the upper branch (II) are plotted in Fig. 14. We see that up to 30% phase squeezing can be obtained in some regions of the upper branch. It again corresponds to bright squeezing.

In Fig. 15, another kind of bistable behavior is exhibited with $G=1.0$, $D=0.2$, $\delta=7.0$, and $\tilde{\alpha}=12$. The stable and phase-locked region for the lower branch(I) starts from $C_L=4.57$ to $C_{\rm th}=5.32$. Unlike the previous two cases, now there is population inversion. In Fig. 16, the corresponding phase noises are plotted for the lower and upper branch, respectively. As we can see, close to 25% phase squeezing has been obtained in the upper branch with the population inversion. This is in contrast to Ref. [8] where the bright squeezing with the population inversion is achieved by introducing an additional lower level and to Ref. [9] where one makes use of a fast intermediate relay level. Here we only need to adjust the cavity detuning, atomic detuning, and other parameters to meet the requirement.

V. CONCLUSIONS

We have studied the nonlinear theory of the two-photon laser with initial atomic coherence from a set of nonlinear equations for the moments derived from the Fokker-Planck equation. First, we analyzed the steady-state operation and bistable behavior of the system. Similar to the one-photon laser with initial atomic coherence, our results showed that, below threshold, the system can exhibit the following features: bistability (hysteresis cycle) and lasing without population inversion occurs and phase can be locked to a particular value. We also showed that in certain cases, a Hopf bifurcation takes place. Below the Hopf bifurcation point, the system is unstable. The time-dependent behavior of the intensity and phase in the unstable region consists of periodic oscillations. Furthermore, we have shown that, for certain parameters, even the tristability can be found. We have also studied the field dynamics. We find that the time-dependent behavior of laser intensity in the unstable regimes is oscillatory (quasiperiodic), and show that there is a stable limit cycle in the phase plane of the quadratures.

Next, we investigated the noise quenching and squeezing in the bistability region. Besides showing that phase noise can be squeezed on the lower branch, we find that the phase squeezing persists for the upper branch even with the population inversion. We thus obtain a bright squeezing source which is compatible with population in-

version in a simple two-photon CEL. This is, perhaps, the most interesting finding of the paper. Processes that are commonly used to generate squeezed states usually permit the generation of the squeezed vacuum state, i.e., the mean of the amplitude is zero. Here we have a process which, in principle, can lead to the generation of a squeezed coherent state, i.e., a state with nonvanishing mean for the amplitude. It should be emphasized that this feature persists on a finite portion of the upper branch above threshold with the magnitude of phase squeezing up to 30%.

ACKNOWLEDGMENTS

This research was supported by a grant of the Office of Naval Research (grant number N00014-92-J-1233) and by a grant from the City University of New York under the PSC-CUNY Research Award Program.

[1] For a recent contribution see, e.g., T. Carty and M. Sargent III, Phys. Rev. A **42**, 2817 (1990), and references therein. Earlier works, in particular, included M. O. Scully, Phys. Rev. Lett. **55**, 2802 (1985) and N. Lu and J. Bergou, Phys. Rev. A **40**, 237 (1989).

[2] J. Bergou, J. Zhang, and A. Hourri, Phys. Rev. A **50**, 4188 (1994).

[3] H. P. Yuen, Phys. Rev. A **13**, 226 (1976).

[4] L. A. Lugiato and G. Strini, Opt. Commun. **41**, 447 (1982); M. D. Reid and D. F. Walls, Phys. Rev. A **28**, 332 (1983).

[5] M. Brune, J. M. Raimond, and S. Haroche, Phys. Rev. A **35**, 154 (1987); L. Davidovich, J. M. Raimond, M. Brune, and S. Haroche, *ibid.* **36**, 377 (1987).

[6] M. O. Scully, K. Wódkiewicz, M. S. Zubairy, J. Bergou, N. Lu, and J. Meyer ter Vehn, Phys. Rev. Lett. **60**, 1832 (1988).

[7] J. Bergou, N. Lu, and M. O. Scully, Opt. Commun. **73**, 57 (1989).

[8] J. Bergou, C. Benkert, L. Davidovich, M. O. Scully, S. Y. Zhu, and M. S. Zubairy, Phys. Rev. A **42**, 5544 (1990).

[9] S. M. Dutra and L. Davidovich, Phys. Rev. A **49**, 2986 (1994).

[10] N. Lu, F-X. Zhao, and J. Bergou, Phys. Rev. A **39**, 5189 (1989).

[11] N. Lu and S. Y. Zhu, Phys. Rev. A **40**, 5735 (1989).

[12] M. Sargent III, M. O. Scully, and W. E. Lamb, Jr., *Laser Physics* (Addison-Wesley, Reading, MA, 1974).

[13] M. Xiao and S. Jin, Phys. Rev. A **45**, 483 (1992); S. Jin and M. Xiao, Phys. Rev. A **49**, 499 (1994).

[14] K. Wang and Y. Wang, J. Opt. Soc. Am. B **10**, 2130 (1993).